



OPEN

Development of a non-radiometric method for measuring the arterial input function of a ^{11}C -labeled PET radiotracer

H. Umesha Shetty¹✉, Sami S. Zoghbi¹, Cheryl L. Morse¹, Aneta Kowalski¹, Jussi Hirvonen², Robert B. Innis¹ & Victor W. Pike¹

Positron emission tomography (PET) uses radiotracers to quantify important biochemical parameters in human subjects. A radiotracer arterial input function (AIF) is often essential for converting brain PET data into robust output measures. For radiotracers labeled with carbon-11 ($t_{1/2} = 20.4$ min), AIF is routinely determined with radio-HPLC of blood sampled frequently during the PET experiment. There has been no alternative to this logistically demanding method, neither for regular use nor validation. A ^{11}C -labeled tracer is always accompanied by a large excess of non-radioactive tracer known as carrier. In principle, AIF might be obtained by measuring the molar activity (A_m ; ratio of radioactivity to total mass; Bq/mol) of a radiotracer dose and the time-course of carrier concentration in plasma after radiotracer injection. Here, we implement this principle in a new method for determining AIF, as shown by using [^{11}C]PBR28 as a representative tracer. The method uses liquid chromatography-tandem mass spectrometry for measuring radiotracer A_m and then the carrier in plasma sampled regularly over the course of a PET experiment. A_m and AIF were determined radiometrically for comparison. The new non-radiometric method is not constrained by the short half-life of carbon-11 and is an attractive alternative to conventional AIF measurement.

Positron emission tomography (PET) is a uniquely valuable molecular imaging modality for noninvasively exploring physiology and biochemistry in health and disease^{1,2}, and has an expanding role in drug development³ and medical diagnosis⁴. PET has notable importance for neuropsychiatric research both for the study of pathophysiology and for drug development. Appropriately designed radiotracers⁵ permit sensitive imaging and quantification of many of the proteins in brain⁶ that are implicated in neuropsychiatric⁷, neurological⁸, and neurodegenerative disorders⁹, as well as substance dependence¹⁰. These proteins include various neurotransmitter receptors, transporters, enzymes, and amyloid plaques³. PET radiotracers may also be used to verify protein target engagement by experimental drugs and how target engagement varies with dosing regimen¹¹. Such information can be critical for establishing meaningful clinical trials. Short-lived carbon-11 ($t_{1/2} = 20.4$ min) or fluorine-18 ($t_{1/2} = 110$ min) are the two most commonly used radionuclides for labeling radiotracers for PET imaging of brain⁵.

Typically, in each PET scanning session, measurement of the radiometabolite-corrected arterial input function (AIF) of the radiotracer is required for use in conjunction with a biomathematical model to robustly quantify a radiotracer target within brain¹². Nearly all PET radiotracers generate radiometabolites in plasma⁵. The AIF is the time-course of non-metabolized radiotracer in plasma. Virtually all AIF measurement has been based on a single methodology, namely fast radio-high performance liquid chromatography (radio-HPLC) separation of the parent radiotracer from radiometabolites in plasma from multiple blood samples taken serially throughout a PET scanning session for radiometric quantification. When imaging with a ^{11}C -labeled PET tracer, the time available for measuring AIF by this means is severely constrained to a few half-lives (typically ~ 90 min). This is very logistically demanding. Whereas the dose of a radiotracer administered to a human subject (~ 750 MBq) is measured with an ionization chamber, the low levels of radioactivity found in plasma samples (of the order of kBq) are typically measured with a sensitive γ -counter. The accuracy of radioactivity measured with an ionization chamber or γ -counter depends, among other factors, on the surrogate radioisotope(s) used to calibrate

¹Molecular Imaging Branch, National Institute of Mental Health, National Institutes of Health (NIMH/NIH), Building 10, Room B3C351, 10 Center Drive, MSC 1003, Bethesda, MD 20892, USA. ²Department of Radiology and Turku PET Centre, University of Turku and Turku Central Hospital, 20520 Turku, Finland. ✉email: shettyu@mail.nih.gov

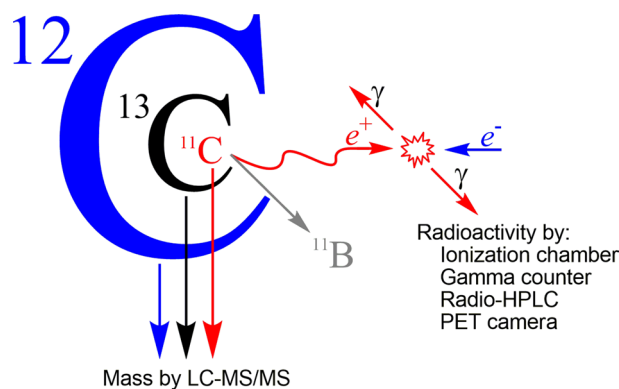


Figure 1. Relative abundances of carrier ($[^{12}\text{C}]_i + [^{13}\text{C}]_i$) and carbon-11 ($[^{11}\text{C}]_i$) species in a ^{11}C -labeled tracer: $[^{12}\text{C}]_i$ 98.9%; $[^{13}\text{C}]_i \sim 1.1\%$; and $[^{11}\text{C}]_i$ typically $< 0.1\%$. In this report, LC-MS/MS was used to measure these three species in order to derive the relationship between tracer mass (through activity derived from Avogadro's number and decay constant) and radioactivity.

the instruments^{13,14}. Notably, no alternative method has ever been available to validate AIFs measured with the conventional radiometric technique. A method for AIF measurement that avoids the severe time constraint imposed by fast decaying radioactivity would be invaluable.

A ^{11}C -labeled PET radiotracer is always accompanied by a matching non-radioactive tracer known as carrier. Although the carrier mass is typically small (< 5 nmol) in any administered radiotracer dose, it is always much larger than the mass of the radiotracer, usually by about three orders of magnitude. In principle, AIF may be obtained by measuring the molar activity (A_m ; ratio of radioactivity to combined mass of tracer and carrier; Bq/mol) of a radiotracer dose and the time-course of the very low concentrations of carrier in plasma after radiotracer injection.

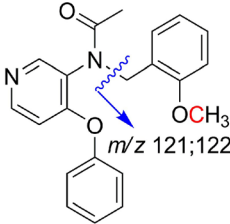
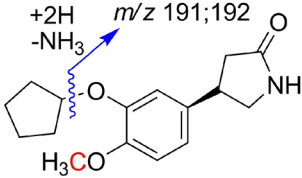
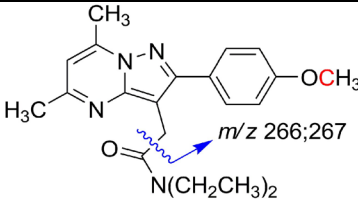
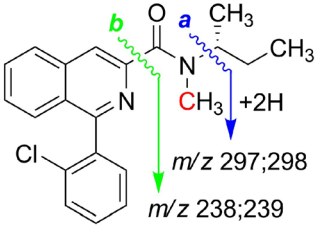
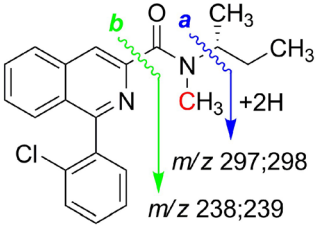
An earlier study from our laboratory demonstrated that liquid chromatography-tandem mass spectrometry (LC-MS/MS) has sufficient sensitivity to detect not only the non-radioactive isotopologues (i.e., ^{12}C and ^{13}C species) in a ^{11}C -labeled tracer but also the relatively low mass radioactive isotopologue (i.e., the ^{11}C species)¹⁵. Here, in this study, we further explored the use of sensitive LC-MS/MS to measure each of the three carbon isotopologues in a PET radiotracer dose, which we here denote $[^{11}\text{C}]_i$, $[^{12}\text{C}]_i$, and $[^{13}\text{C}]_i$, (Fig. 1), and the application of such measurements to human plasma samples for AIF determination. We furthermore compared the resultant A_m and AIF data with those determined by the conventional radiometric method for the same ^{11}C -labeled radiotracer, using $[^{11}\text{C}]$ PR28 as the principal example.

To develop an LC-MS/MS method for AIF determination, we needed to show that LC-MS/MS has (1) sufficient sensitivity to accurately measure the ratio of all three isotopologues in a radiotracer dose, (2) adequate sensitivity and specificity to measure the low level of carrier from the radiotracer in human plasma after intravenous administration of the radiotracer at a useful molar activity, especially over the whole time course of PET imaging (typically 90 min), and (3) that the obtained AIF is reliable and accurate. We performed detailed experiments to establish these aims.

Results

LC-MS/MS investigation of the carrier in ^{11}C -labeled tracers: ^{13}C to ^{12}C ratio at the radiolabeling site and dependence of this ratio on A_m . As part of method development, we set out to measure the ratio of ^{13}C to ^{12}C in the carrier of some ^{11}C -labeled tracers to determine whether there was any variability that might impact on the proposed use of LC-MS/MS for measuring A_m and AIF. We showed that we could measure simultaneously all three isotopologues, $[^{11}\text{C}]_i$, $[^{12}\text{C}]_i$, and $[^{13}\text{C}]_i$, in radiotracers with high A_m values and, two isotopologues, $[^{11}\text{C}]_i$ and $[^{13}\text{C}]_i$, when A_m is in low to moderate range. The ratio of ^{13}C to ^{12}C in the natural environment is about 1.1% but shows small variations that depend on carbon source¹⁶. For the determination of A_m values, we proposed to measure two isotopologues only, $[^{11}\text{C}]_i$, and $[^{13}\text{C}]_i$. This approach avoids detector saturation with the much more abundant $[^{12}\text{C}]_i$, especially for samples with A_m at the lower end of the normal range. To calculate the amount of $[^{12}\text{C}]_i$ from a measurement of $[^{13}\text{C}]_i$, their exact ratio in a sample of the compound would need to be known. This ratio was first measured in natural abundance reference compounds for four of the studied PET radiotracers (specifically, three TSPO radiotracers— $[^{11}\text{C}]$ PBR28¹⁷, $[^{11}\text{C}]$ (R)-PK11195¹⁸, and $[^{11}\text{C}]$ DPA713¹⁹—and one cyclic adenosine monophosphate (cAMP) phosphodiesterase-4 (PDE-4) radiotracer, $[^{11}\text{C}]$ (R)-rolipram²⁰). The obtained values were within the expected range of about 1.1% per carbon atom in a measured product ion (reference standards, Table 1).

However, when this method was applied to the carrier present in prepared radiotracer doses, we observed $[^{13}\text{C}]_i$ to $[^{12}\text{C}]_i$ ratios that were well above the normal range for natural abundance (Table 1). These findings showed that ^{13}C enrichment had occurred during radiotracer production, which we now attribute to a known nuclear reaction, $^{14}\text{N}(p,2n)^{13}\text{C}$, that would co-exist with the $^{14}\text{N}(p,\alpha)^{11}\text{C}$ reaction during the cyclotron production of carbon-11 through irradiation of nitrogen with 16 MeV protons (see “Discussion” section)²¹. In our production setting, the A_m value of a PET radiotracer strongly reflects the amount of radioactivity produced during

Radiotracer	Ions measured (<i>m/z</i>)	Number of carbons in product ion	A_m (GBq/ μ mol) ^a	Ratio of [¹³ C] _i to [¹² C] _i (%) ^b
 PBR28	121, 122	8	367	9.12 ± 0.08 ^c
			876	9.89 ± 0.02
 (R)-Rolipram	191, 192	11	178	12.48 ± 0.07 ^c
			1194	13.12 ± 0.07
 DPA713	266, 267	16	433	18.72 ± 0.04 ^c
			566	19.91 ± 0.04
 (R)-PK11195	238, 239 ^e	15	483	17.10 ± 0.16 ^c
			618	17.09 ± 0.12
 (R)-PK11195	297, 298 ^d	17	483	19.98 ± 0.18 ^c
			618	20.94 ± 0.21

^aDetermined with radio-HPLC.

^bMean ± SD of four LC-MS/MS measurements; ratio includes minor contribution from the natural abundances of ²H, ¹⁷O, and ¹⁵N.

^c[¹³C]_i to [¹²C]_i ratio for the reference non-radioactive compound.

^dFrom fragmentation a.

^eFrom fragmentation b.

Table 1. Ratios of [¹³C]_i to [¹²C]_i in the carrier of four ¹¹C-labeled PET radiotracers produced at two different A_m values, and in the respective reference compounds. The red carbon denotes the site that is labeled with carbon-11 in each radiotracer. ^aDetermined with radio-HPLC. ^bMean ± SD of four LC-MS/MS measurements; ratio includes minor contribution from the natural abundances of ²H, ¹⁷O, and ¹⁵N. ^c[¹³C]_i to [¹²C]_i ratio for the reference non-radioactive compound. ^dFrom fragmentation a. ^eFrom fragmentation b.

cyclotron irradiation, which in turn depends on the integrated proton beam current (μ A × min)²². Consequently, we predicted that the [¹³C]_i to [¹²C]_i ratio would increase with the measured A_m value of the ¹¹C-labeled tracer. In each of four radiotracers, when measuring the fragment ion that contained the radiolabeling site in two separately prepared doses, the [¹³C]_i to [¹²C]_i ratio was higher in the dose that had the higher A_m value (determined radiometrically) (Table 1). One radiotracer (R)-PK11195 gave abundant product ions (*m/z* 238; 239) that lacked the ¹¹C-labeling site (i.e., lacked the amido *N*-methyl group). The [¹³C]_i to [¹²C]_i ratio for these ions was found to be in the range of natural abundance and invariant with the A_m value of the radiotracer preparation (Table 1), thereby affirming that changes in ¹³C-enrichment were confined to the fragment containing the ¹¹C-labeling site.

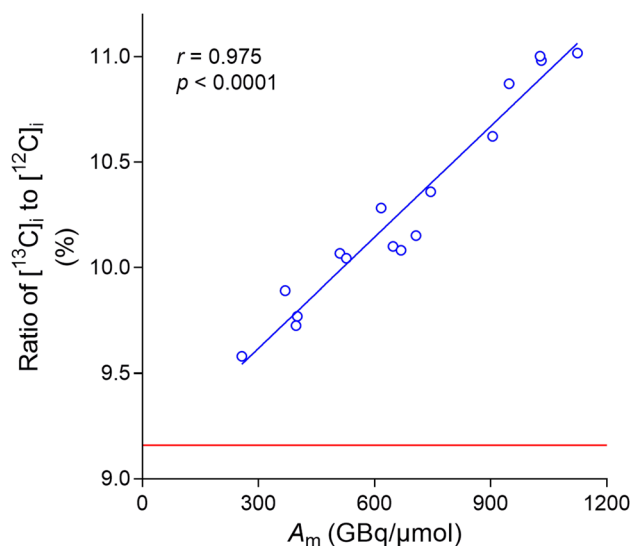


Figure 2. The percentage ratio of $[^{13}\text{C}]_i$ to $[^{12}\text{C}]_i$ in carrier increased linearly with A_m value (determined by LC–MS/MS) for $[^{11}\text{C}]$ PBR28 preparations. The red line represents the mean value of the ratio in reference PBR28.

The data from Table 1 were used to plot the increase in the ratio of $[^{13}\text{C}]_i$ to $[^{12}\text{C}]_i$ for the carrier in all eight radiotracer productions versus A_m value. These values and the corresponding A_m values were found to be strongly correlated ($r = 0.895$; $p < 0.003$) (Supplementary Fig. S1).

Determination of radiotracer A_m by LC–MS/MS alone. A_m values for $[^{11}\text{C}]$ PBR28 preparations were measured with LC–MS/MS by isolating and monitoring the isotopologue pair, $[^{11}\text{C}]_i$ and $[^{13}\text{C}]_i$, as previously described for ^{11}C -labeled tracers¹⁵. In that study, the ratio of $[^{13}\text{C}]_i$ to $[^{12}\text{C}]_i$ was taken to be the fixed value measured in reference PBR28. Here, in a refinement of this procedure, the ratio of $[^{13}\text{C}]_i$ to $[^{12}\text{C}]_i$ in the carrier of each $[^{11}\text{C}]$ PBR28 preparation was used to calculate the ^{12}C -peak area from which A_m values could then be derived. In the case of a few $[^{11}\text{C}]$ PBR28 preparations, where the A_m values were relatively high (905–1124 GBq/ μ mol), LC–MS/MS successfully isolated and monitored all three carbon isotopologues simultaneously ($[^{11}\text{C}]_i$, $[^{12}\text{C}]_i$, and $[^{13}\text{C}]_i$) (Supplementary Fig. S2). This direct measurement of all three types of isotopologue yielded A_m values that closely matched those obtained by measuring only the two isotopologues $[^{11}\text{C}]_i$ and $[^{13}\text{C}]_i$. Therefore, measurement of $[^{11}\text{C}]_i$ and $[^{13}\text{C}]_i$ alone plus a separate measurement of the ^{13}C to ^{12}C ratio in a radiotracer dose sufficed to provide an accurate A_m value.

Plot of $[^{13}\text{C}]_i$ to $[^{12}\text{C}]_i$ ratio versus A_m (by LC–MS/MS) for $[^{11}\text{C}]$ PBR28. A_m values, including the ratio of $[^{13}\text{C}]_i$ to $[^{12}\text{C}]_i$, were determined in 16 preparations of $[^{11}\text{C}]$ PBR28. Variations in radiosynthesis time were negligible (36.3 ± 0.82 min; mean \pm SD; $n = 16$) and dose radioactivity was therefore decay-corrected to the end of each synthesis. As a control, the ratio of $[^{13}\text{C}]_i$ to $[^{12}\text{C}]_i$ was also measured in reference (natural abundance) PBR28 on each occasion of radiotracer analysis. The ratios of $[^{13}\text{C}]_i$ to $[^{12}\text{C}]_i$ for $[^{11}\text{C}]$ PBR28 preparations correlated strongly with A_m values determined with LC–MS/MS ($r = 0.975$; $p < 0.0001$; $n = 16$) (Fig. 2). The Y-axis intercept of 9.09% ($A_m = 0$) for this curve was almost identical to the mean ratio of $[^{13}\text{C}]_i$ to $[^{12}\text{C}]_i$ measured for reference PBR28 ($9.16 \pm 0.05\%$; mean \pm SD; $n = 16$; represented by the red line in Fig. 2). The small standard deviations in the latter value and those in Table 1 demonstrate the high precision with which such ratios could be determined with LC–MS/MS.

Comparison of LC–MS/MS and radiometric methods for measuring A_m . The A_m values of each of 15 preparations of $[^{11}\text{C}]$ PBR28 were measured in three different ways: with LC–MS/MS alone (Method 1) ; with carrier measured with LC–MS/MS and radioactivity measured in a calibrated γ -counter (Method 2), and with the conventional radiometric method based on radioactivity dose measured in an ionization chamber and carrier measured with HPLC (Method 3) (Supplementary Methods). A scatter plot of the percentage difference between the A_m values measured with LC–MS/MS alone and each of the two radiometric methods is displayed in Supplementary Fig. S3. When compared with LC–MS/MS (Method 1), measurement with an ionization chamber (Method 2) gave $1.5 \pm 10.1\%$ lower A_m values, and measurement with a γ -counter (Method 3) gave $33.2 \pm 3.3\%$ higher A_m values.

Comparison of radioactivity measurements made with LC–MS/MS with those of γ -counter. Radioactivity in a sample of $[^{11}\text{C}]$ PBR28 was measured with a calibrated γ -counter. The carrier $[^{12}\text{C}]_i$ in the same sample was then quantified with LC–MS/MS using an internal standard of $[^{13}\text{C},^2\text{H}_3]$ PBR28 to calibrate the LC–MS/MS response. Radioactivity based on the mass of $[^{11}\text{C}]_i$ was calculated using the concentra-

$[^{11}\text{C}]\text{PBR28}$ preparation	Carrier by LC-MS/MS (pmol) ^a	A_m by LC-MS/MS (GBq/ μmol) ^b	Radioactivity by		Difference in radioactivity (%) ^d
			LC-MS/MS (kBq) ^c	γ -counter (kBq)	
1	15.2	200.4	3040	4019	32.2
2	5.56	631.1	3510	4817	37.2
3	12.1	383.5	4645	6310	35.8
4	1.75	904.9	1580	2092	32.4
5	2.90	1124	3261	4249	30.3
6	2.95	1028	3036	4150	36.7

Table 2. Comparison of $[^{11}\text{C}]\text{PBR28}$ radioactivity data from γ -counter and from LC-MS/MS. ^aMeasured using $[^{13}\text{C},^2\text{H}_3]\text{PBR28}$ as an internal standard. ^b A_m value by LC-MS/MS of $[^{11}\text{C}]_i$ and $[^{13}\text{C}]_i$ (1–3), and of the triad $[^{11}\text{C}]_i$, $[^{12}\text{C}]_i$, and $[^{13}\text{C}]_i$ (4–6). ^cRadioactivity calculated from the A_m and carrier, each measured with LC-MS/MS. ^dFrom that determined with LC-MS/MS.

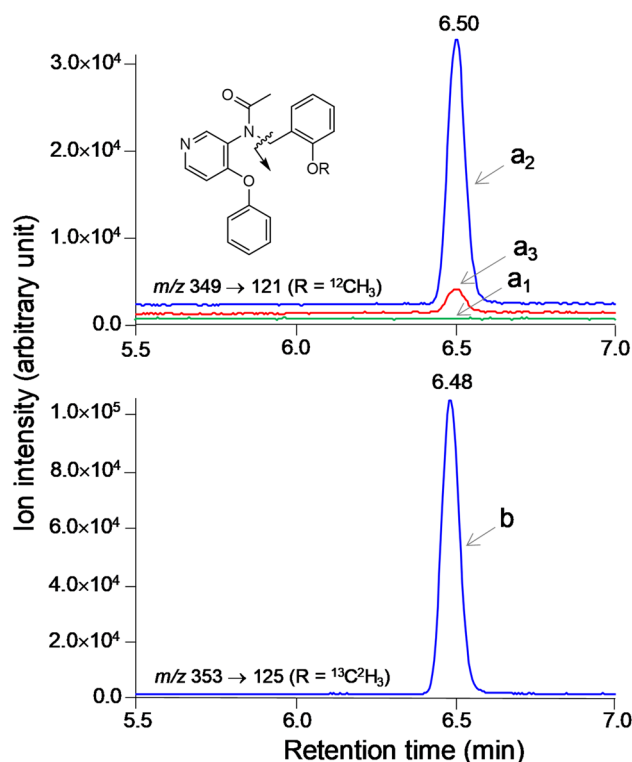


Figure 3. LC-MS/MS ion chromatograms ($m/z=121$; $[^{12}\text{C}]_i$) for carrier PBR28 in arterial plasma sampled from a human subject injected intravenously with $[^{11}\text{C}]\text{PBR28}$ for PET imaging. a_1 : baseline. Peaks a_2 and a_3 : carrier PBR28 peaks at 10 min (71.8 pM) and 90 min (6.34 pM) after injection, respectively. Peak b in ion chromatogram ($m/z=125$) is from the analogous transition in the internal standard, $[^{13}\text{C},^2\text{H}_3]\text{PBR28}$ (284 pM).

tion of the carrier and the A_m value of $[^{11}\text{C}]\text{PBR28}$ determined with LC-MS/MS. Measurement with a γ -counter gave $31.8 \pm 3.8\%$ ($n=24$) higher radioactivity values than LC-MS/MS. Data from the analysis of six $[^{11}\text{C}]\text{PBR28}$ preparations are shown in Table 2. The substantial difference between the radioactivity obtained by direct counting and through the mass of $[^{11}\text{C}]_i$ was independent of the A_m value (200–1028 GBq/ μmol) and also independent of whether two isotopologues ($[^{11}\text{C}]_i$ and $[^{13}\text{C}]_i$) or three isotopologues ($[^{11}\text{C}]_i$, $[^{12}\text{C}]_i$ and $[^{13}\text{C}]_i$) were analyzed. Thus, differences in radioactivity estimates from γ -counting and LC-MS/MS accounted for all the A_m discrepancies shown in Supplementary Fig. S3b.

LC-MS/MS of carrier in human plasma. By using $[^{13}\text{C},^2\text{H}_3]\text{PBR28}$ as an internal standard, a LC-MS/MS method was developed to quantify the very low amounts of PBR28 carrier in the plasma of eight human subjects who had been injected intravenously with $[^{11}\text{C}]\text{PBR28}$ for PET scanning. Figure 3 shows ion chromatograms from the analysis of plasma at baseline, and at 10 and 90 min after intravenous injection of $[^{11}\text{C}]\text{PBR28}$ (710 MBq; A_m : 383.5 GBq/ μmol) in one subject. The plasma matrix did not interfere with the ionization or detection of carrier PBR28 or of the internal standard, and no interfering peak was observed in the ion chroma-

A_m (GBq/ μ mol) ^a	Time after injection (min)	Carrier concentration (pM)		
		Radiometric ^b		LC-MS/MS
		A	B	
138.6	1.25	2349	1726	1790
	2.50	416.8	306.2	303.9
	20.00	52.20	38.36	36.02
	59.98	29.81	21.90	21.83
200.4	1.23	1551	1173	1097
	2.48	304.6	230.4	214.6
	20.18	50.84	38.46	32.31
	60.00	17.41	13.17	11.76
385.9	1.25	773.8	599.9	594.1
	2.50	140.1	108.6	103.7
	20.00	16.48	12.77	11.10
	60.00	7.288	5.649	5.158

Table 3. Carrier PBR28 concentration (pM) in arterial plasma after [¹¹C]PBR28 injection. ^aDetermined with LC-MS/MS for each radiometric and LC-MS/MS method. ^bFrom radiometric measurement before (A) and after (B) the correction of radioactivity (for the systematic difference between LC-MS/MS and γ -counter measures).

tograms. The measured ratios of carrier to internal standard peak area gave the true concentrations of carrier PBR28 from the linear calibration curve (Supplementary Fig. S4).

LC-MS/MS measurement for AIF determination. The A_m values of [¹¹C]PBR28 doses administered to three different human subjects for PET imaging were measured with LC-MS/MS. These values were used to convert arterial plasma [¹¹C]PBR28 radioactivity from conventional AIF measurements at four timepoints into picomolar concentrations of carrier PBR28. This allowed the two datasets (radiometric and LC-MS/MS) to be compared. The plasma concentration of carrier PBR28 decreased as the A_m value of the injected radiotracer increased, as would be expected for similar administered amounts of radioactivity per weight of subject. Plasma concentrations of carrier PBR28 calculated from radiometric measurement of [¹¹C]PBR28 radioactivity were higher than those measured with LC-MS/MS. After correcting for the systematic difference between measurements, the carrier PBR28 concentrations determined by radiometric and LC-MS/MS methods were highly comparable (Table 3), including those at very low levels of carrier concentration (~5 pM). Further experiments showed that the LC-MS/MS method had adequate sensitivity to measure [¹¹C]PBR28 in plasma at 23 timepoints for up to 90 min following intravenous injection of the radiotracer at different molar activities.

Comparisons of AIFs for [¹¹C]PBR28 from LC-MS/MS and radiometric methods. The carrier PBR28 concentrations in plasma samples measured with LC-MS/MS were transformed into radioactivity data using A_m measured with LC-MS/MS. An example of a log-linear plot of plasma [¹¹C]PBR28 radioactivity versus time (i.e., AIF) from the new LC-MS/MS method and the conventional radiometric method for a human subject injected with [¹¹C]PBR28 at a moderately high A_m value (i.e., with low carrier) is illustrated in Fig. 4a. In this example, and in seven other PET experiments with [¹¹C]PBR28, the log-linear plots of AIFs from LC-MS/MS ran nearly parallel below the AIFs obtained via the conventional radiometric method. After correcting the plasma radioactivity measured with the γ -counter for the systematic difference between the methods (as described above, see Supplementary Fig. S3), the AIF measured with LC-MS/MS became virtually superimposed with that measured radiometrically (Fig. 4b) for each example. AIF plots from radiometric and LC-MS/MS measurements for human subjects administered with [¹¹C]PBR28 of a low A_m of 141.8 GBq/ μ mol and a high A_m of 631.1 GBq/ μ mol are shown in Fig. 4c,d, respectively.

To examine the impact of different types of AIF measurement on the input function for kinetic modeling of PET data, we compared areas under the curve (AUCs) for the plasma time-activity curves. On average, AUC calculated from LC-MS/MS was 31% lower than that calculated with the radiometric method ($t = -11.9$, $p < 0.001$), and 8% lower than that calculated with the corrected radiometric method ($t = -6.0$, $p < 0.001$) (Table 4). VAR, Pearson correlation coefficient, and ICC, were respectively 37%, 0.97, and 0.07 for LC-MS/MS versus direct radiometric method, and 8%, 0.99, and 0.91 for LC-MS/MS versus the corrected radiometric method.

Discussion

This study assessed the feasibility of using LC-MS/MS for measuring AIF in human subjects undergoing PET scanning with a ¹¹C-labeled radiotracer. LC-MS/MS analysis was found to provide a convenient and sensitive method for measuring the AIF of a ¹¹C-labeled tracer without measuring its radioactivity. This method can be performed on multiple blood samples without the time and logistical constraints of the conventional radiometric method. The A_m measured during the production of a radiotracer may be used to transform plasma carrier concentrations into AIF radioactivity data.

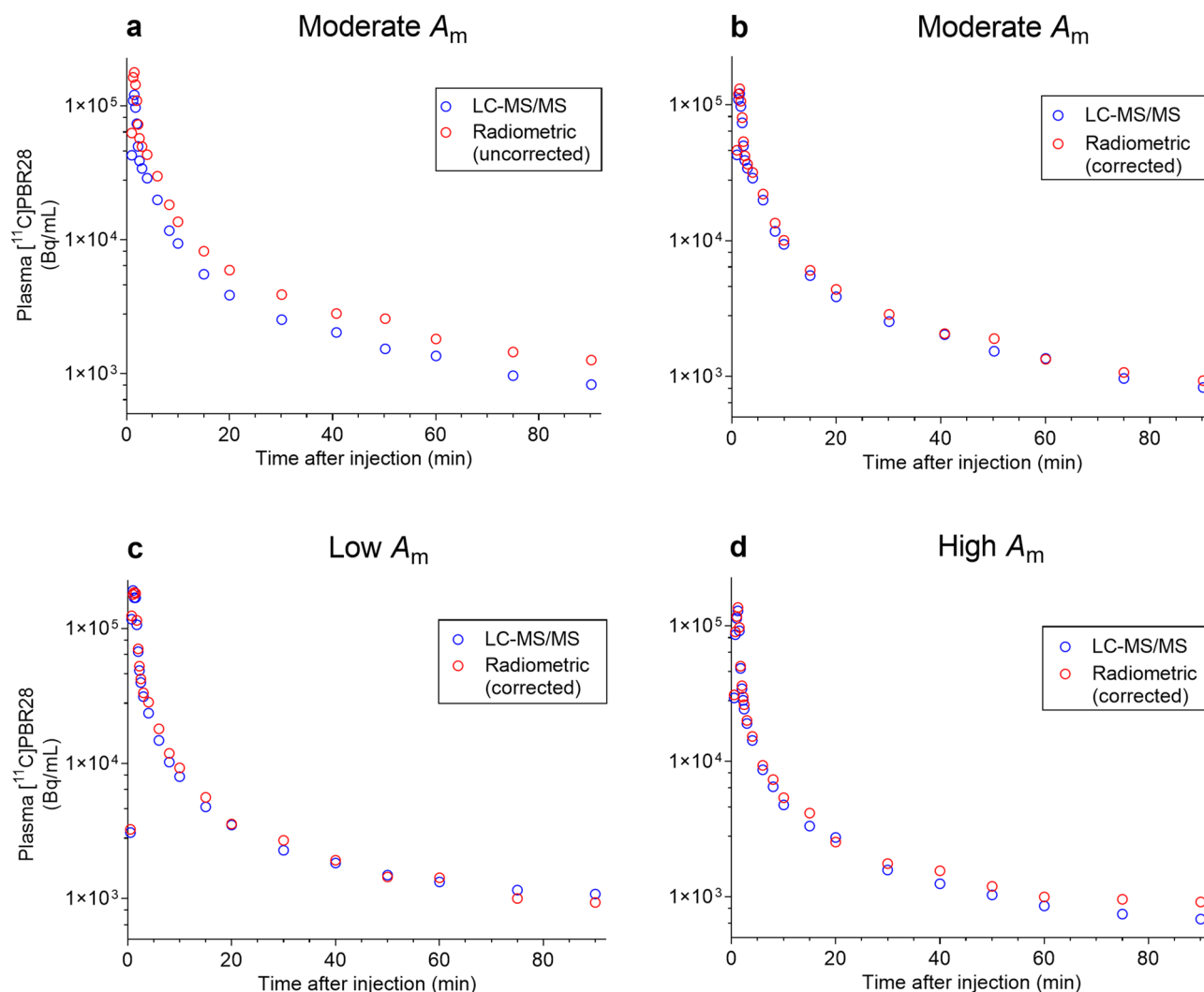


Figure 4. Examples of AIFs determined in human subjects with radiometric and LC-MS/MS methods for $[^{11}\text{C}]\text{PBR28}$. (a) AIFs for one subject injected with $[^{11}\text{C}]\text{PBR28}$ (10.1 MBq/kg; injected mass 92 pmol/kg, i.v.) with an A_m of 383.5 GBq/ μmol . The AIF from radiometric method is without correction of γ -counter measured radioactivity for the systematic difference with LC-MS/MS. (b) Comparisons of AIFs from the same experiment after correction of γ -counter measured radioactivity. (c) AIFs from radiometric (corrected) and LC-MS/MS measurements in another human subject injected with $[^{11}\text{C}]\text{PBR28}$ (10.7 MBq/kg; injected mass 229 pmol/kg, i.v.) at a lower A_m of 141.8 GBq/ μmol . (d) AIFs from the same methods in a subject injected with radiotracer (9.5 MBq/kg; injected mass 44 pmol/kg, i.v.) at a higher A_m of 631.1 GBq/ μmol . Note all data are for unchanged radiotracer alone (i.e., radiometabolites are excluded).

During the LC-MS/MS analysis of the triad, $[^{11}\text{C}]_i$, $[^{12}\text{C}]_i$, and $[^{13}\text{C}]_i$ in all four tested radiotracers, we observed a higher $[^{13}\text{C}]_i$ to $[^{12}\text{C}]_i$ ratio than in the respective non-radioactive standard (Table 1). The MS/MS technique demonstrated that ^{13}C -enrichment had occurred in the carrier at the same position that had been labeled with carbon-11 during radiotracer synthesis. As clearly shown for $[^{11}\text{C}]\text{PBR28}$, the degree of isotopic enrichment correlated with A_m value. Therefore, the augmented $[^{13}\text{C}]_i$ to $[^{12}\text{C}]_i$ ratio was not due to an isotope effect in the synthesis or purification of the radiotracer. The carbon-11 for labeling each radiotracer was produced by the $^{14}\text{N}(p,\alpha)^{11}\text{C}$ reaction on nitrogen with a 16 MeV beam of protons which degrade in energy on progressing through the gas target. An explanation for the A_m -related ^{13}C -enrichment is the co-occurrence of the $^{14}\text{N}(p,2p)^{13}\text{C}$ reaction. For irradiations of nitrogen gas with 13.2 MeV protons, the $^{14}\text{N}(p,2p)^{13}\text{C}$ reaction has a total cross section of 74.2 mb (millibarn) which is very similar to that for the $^{14}\text{N}(p,\alpha)^{11}\text{C}$ reaction (68.9 mb)²³. Therefore, the mass of generated carbon-13 is expected to be similar to the mass of carbon-11 produced. For a typical 40-min irradiation producing about 75 GBq of carbon-11, this amount would be about 10 nmol, or roughly enough to explain the ^{13}C -enrichment seen for carrier in doses of $[^{11}\text{C}]\text{PBR28}$.

The A_m value of a radiotracer needs to be determined accurately in order to derive mass of carrier from radioactivity or vice versa. A previous study from our laboratory reported an MS/MS technique for isolating $[^{11}\text{C}]_i$ and $[^{13}\text{C}]_i$ to measure the A_m values for ^{11}C -labeled tracers¹⁵. Each A_m value was calculated using a constant $[^{13}\text{C}]_i$ to $[^{12}\text{C}]_i$ ratio that had been measured for the reference natural abundance ligand. In the present study, the

Human subject	AUCs (kBq × min/mL)			Difference (%) ^b	
	LC–MS/MS	Radiometric ^a		A	B
		A	B		
1	328	470	356	36	8
2	308	485	351	44	13
3	329	437	339	28	3
4	332	465	342	33	3
5	334	500	365	40	9
6	460	686	505	39	9
7	336	517	380	42	12
8	518	730	559	34	8
Mean ± SD	368 ± 77	536 ± 109	399 ± 84	37 ± 5.3	8.1 ± 3.6
RSD (%)	21	20	21		

Table 4. AUCs (kBq × min/mL) for the plasma time-activity curves from LC–MS/MS and radiometric measurements. ^aAUCs from radiometric measurements before (A) and after (B) the correction of radioactivity (for the systematic difference between LC–MS/MS and γ -counter measures). ^bBetween the AUC from LC–MS/MS and that from the radiometric method for AUC dataset A and AUC dataset B.

A_m value for [¹¹C]PBR28 was measured according to the same principle except that the specific [¹³C]_i to [¹²C]_i ratio of the carrier in the radiotracer was used for greater accuracy.

The sensitivity and dynamic range of MS/MS was found to be adequate to measure all three isotopologues in [¹¹C]PBR28 with relatively high A_m values (~ 1000 GBq/μmol) (Supplementary Fig. S2). Such radiotracer preparations allowed injection of more diluted sample into the LC–MS/MS and thus measurement of carrier [¹²C]_i without saturating the detector. The A_m values determined from [¹¹C]_i and [¹³C]_i, as well as the [¹³C]_i to [¹²C]_i ratio, were found to be valid because direct measurement of the [¹¹C]_i, [¹²C]_i, and [¹³C]_i triad yielded similar results (Table 2). The A_m value measured with a γ -counter was used to compare these two sets of data.

These findings further demonstrated that the LC–MS/MS technique can isolate and measure very low kBq levels of [¹¹C]_i and, consequently, that this capability can be used to evaluate the accuracy of radioactivity measurements from radiation detectors such as ionization chambers and γ -counters. Building on this work, we compared the A_m values of [¹¹C]PBR28 measured with LC–MS/MS with those determined using an ionization chamber and a γ -counter. The A_m (mean ± SD) value measured by ionization chamber was close to that obtained via LC–MS/MS, whereas that obtained via γ -counter was appreciably higher. Thus, comparing the three sets of A_m data revealed a significant difference in radioactivity estimates between the two commonly used radiometric methods.

Typically, an ionization chamber is calibrated for measuring carbon-11 with a pair of surrogate radioisotope standards, ¹³⁷Cs ($t_{1/2}$ = 30.17 years; β^- , γ 662 keV) and ⁵⁷Co ($t_{1/2}$ = 271.79 days; ϵ , γ 122, 136 keV), and a γ -counter with a different standard, ⁶⁸Ge ($t_{1/2}$ = 270.8 days; decays to ⁶⁸Ga; $t_{1/2}$ = 67.6 min, β^+ , ϵ , γ). Clearly, these surrogate isotopes have decay modes that are very different from those of ¹¹C (β^+ , ~ 99.8%). Moreover, the accuracy of radioactivity measured with an ionization chamber or γ -counter is well known to be influenced by sample volume and geometry effects^{14,24,25}. Studies seeking to measure positron-emitters in ionization chambers have been conducted with fluorine-18 ($t_{1/2}$ = 109.8 min)^{24,25}, but none have used shorter-lived carbon-11. Indeed, we have previously observed in our facility that identical ionization detectors calibrated in the same way with the same surrogate standards can give estimates of carbon-11 radioactivity differing by up to 12%¹⁵. During the course of the present study, we thoroughly investigated whether such differences could be ascribed to detector dead-time and linearity, sample geometry, and volume effects, to the material of the sample container (glass or polypropylene), or to measurement time. None of these factors accounted for the observed differences. These results underscore the role that a sensitive MS/MS technique may play in checking radioactivity measured with radiometric techniques. Notably, the MS/MS technique obviates sample volume and geometry concerns.

In the conventional radiometric measurement of AIF, plasma radioactivity is measured with a γ -counter and then corrected for the contribution of radiometabolites, as determined with radio-HPLC analysis^{17,18} (for radiochromatogram, Supplementary Fig. S5). The accuracy of AIF determined in this manner depends on the calibration of the γ -counter. The AIF data so generated can be compared with those from the LC–MS/MS of the carrier if equivalence between measured radioactivity and mass of [¹¹C]_i has been demonstrated. Here, radioactivity based on the mass of [¹¹C]_i was determined from the A_m and concentration of carrier (from LC–MS/MS) in a sample whose radioactivity had been measured with a γ -counter. The γ -counter measurement gave a higher value. Accordingly, it was necessary to adjust the radioactivity measured with a γ -counter to achieve a meaningful comparison of AIF determined from radiometric and LC–MS/MS methods.

LC–MS/MS, with the use of an internal standard labeled with stable isotopes (¹³C and deuterium), was able to quantify carrier PBR28 in small volumes of plasma (200 μL) taken from human subjects undergoing PET experiments with [¹¹C]PBR28. Calibration of the method used reference PBR28 whose [¹³C]_i to [¹²C]_i ratio is lower than that of carrier PBR28. The unexpectedly skewed [¹³C]_i to [¹²C]_i ratio in the carrier was found to contribute negligible error (< 1%) to measurements of PBR28 concentrations. The LC–MS/MS method was sensitive and specific enough to measure carrier PBR28 up to 90 min after injection of radiotracer with A_m values in the range

of 139 to 631 GBq/ μmol . ^{11}C -Labeled radiotracers are typically administered with molar activities at the lower end of this range. The entire range of quantification was achieved by injecting as little as 1/20th of each plasma sample onto the LC–MS/MS. If using a radiotracer with an exceptionally higher A_m value, quantification could still be achieved by increasing the injection volume, from for example 10 to 25 μL , or concentrating the plasma sample two-fold, although the LC procedure might consequently need some modification. In addition, it is expected that quantification limits would vary with the type of radiotracer carrier being measured.

With regards to measuring AIF for $[^{11}\text{C}]\text{PBR28}$, when the radioactivity was corrected for the difference between radioactivity measured by γ -counter and by LC–MS/MS, the plasma concentration curves from the two methods matched (Fig. 4). The difference likely occurred because LC–MS/MS performs absolute quantification of the carrier whereas the γ -counter measures radioactivity relative to the surrogate radioisotope used for calibration. The radioactivity (Bq) is given by the product of the decay constant of the radionuclide and the number of un-decayed radioactive atoms. Thus, the LC–MS/MS measurement described here is expected to give absolute radioactivity, given that it is derived from the mass of $[^{11}\text{C}]_i$, the decay constant of carbon-11, and Avogadro's number.

The AUCs for plasma time-activity curves from the LC–MS/MS method were $8.1 \pm 3.6\%$ ($n = 8$) lower than those from the radiometric method with corrected radioactivity. Nonetheless, the %RSD of AUCs calculated for 8 subjects was the same for the two methods and showed good correlation (Pearson $r = 0.987$; $p = 0.01$). Thus, the LC–MS/MS method is as reproducible as the radiometric method for measuring AIFs.

Conclusion

The LC–MS/MS of fast-decaying PET radiotracers provides interchangeable mass and radioactivity data and offers the convenience of measuring AIF through the carrier of the radiotracer instead of radioactivity. The method, here exemplified with $[^{11}\text{C}]\text{PBR28}$, circumvents possible radiometabolite interference and error due to volume and geometry effects associated with radiometric measurements. Potentially, this non-radiometric method might allow measurement of AIF on stored plasma samples by analytical service laboratories that perform LC–MS/MS quantifications. In such instances, AIFs in radioactivity unit can be derived from the A_m measured during production of the radiotracer. Taken together, the LC–MS/MS technique poses a convenient, non-radiometric, reproducible, and sensitive method for measuring AIF, deserving of widespread application in the expanding PET imaging field.

Methods

The Supplementary Methods describe: (1) Materials; (2) Radiosynthesis; (3) Measurement of A_m using HPLC and an ionization chamber; (4) Technical aspects of AIF measurement by literature radiometric method; (5) Preparation of PBR28 and $[^{13}\text{C},^2\text{H}_3]\text{PBR28}$ internal standard (IS) stock solutions; (6) Extraction of carrier PBR28 in plasma for LC–MS/MS analysis; and (7) Recovery, matrix effect, stability, and reproducibility for LC–MS/MS quantification of carrier PBR28 in plasma.

A_m of $[^{11}\text{C}]\text{PBR28}$ by LC–MS/MS. An aliquot of a $[^{11}\text{C}]\text{PBR28}$ preparation was diluted with LC mobile phase either 15-fold for measuring $[^{11}\text{C}]_i$ and $[^{13}\text{C}]_i$ or 40-fold for measuring $[^{11}\text{C}]_i$, $[^{12}\text{C}]_i$, and $[^{13}\text{C}]_i$. A sample (5 μL ; $n = 6$ or 3) was injected onto LC–MS/MS (API 5000; Sciex; Redwood City, CA). Analysis was performed using LC method and MS/MS settings already described¹⁵. A second transition, m/z 349 \rightarrow 121, was included in the method requiring acquisition of $[^{11}\text{C}]_i$, $[^{12}\text{C}]_i$, and $[^{13}\text{C}]_i$. In A_m measurements based on acquisition of $[^{11}\text{C}]_i$ and $[^{13}\text{C}]_i$, the ^{13}C peak area of the carrier was converted into the ^{12}C peak area using the ratio of $[^{13}\text{C}]_i$ to $[^{12}\text{C}]_i$ measured in the carrier, where $[^{13}\text{C}]_i$ includes $[^{12}\text{C}]_i$ having a single natural abundance ^2H or ^{17}O atom. A_m was determined from the peak areas of radioactive and carrier species as $(A^*)/(A + A^*) \times A_m^*$, where A^* is the sum of peak areas for $[^{11}\text{C}]_i$ and for the calculated area for the same species containing carbon-13, A is the sum of the peak areas for $[^{12}\text{C}]_i$ and $[^{13}\text{C}]_i$, and A_m^* is the theoretical carrier-free A_m of carbon-11 (3.413×10^{20} Bq/mol, the product of $\ln 2/t_{1/2}$ and Avogadro's number)¹⁵.

Ratio of $[^{13}\text{C}]_i$ to $[^{12}\text{C}]_i$. The MS/MS instrument was tuned with reference ligands (PBR28, (R)-rolipram, DPA713, and (R)-PK11195). A method was set up to acquire $[M + H]^+ \rightarrow$ product ion transitions for $[^{12}\text{C}]_i$ and $[^{13}\text{C}]_i$ (which includes ^{12}C species containing a single ^2H , ^{15}N , or ^{17}O atom of natural abundance) for each carrier, as follows: PBR28, m/z 349/350 \rightarrow 121/122; (R)-rolipram, m/z 276/277 \rightarrow 191/192; DPA713, m/z 367/368 \rightarrow 266/267; and (R)-PK11195, m/z 353/354 \rightarrow 297/298 (a) and 238/239 (b) (Table 1). Radiotracer samples were analyzed after full radioactive decay. Specifically, the sample was diluted (100–500 fold) and injected (5 μL ; $n = 4$) onto the LC–MS/MS. Radiotracer's carrier was chromatographed on a C18 column (2 \times 20 mm, 3 μm ; Phenomenex, Torrance, CA) using a similar water-acetonitrile (10 mM ammonium acetate or 0.2% acetic acid) gradient as previously reported¹⁵. The ratio of peak areas for product ion from $[^{13}\text{C}]_i$ to that from $[^{12}\text{C}]_i$, multiplied by 100, gave the ratio $[^{13}\text{C}]_i$ to $[^{12}\text{C}]_i$ as a % value.

Reference PBR28, (R)-rolipram, DPA713, and (R)-PK11195 were analyzed similarly, and the ratio of $[^{13}\text{C}]_i$ and $[^{12}\text{C}]_i$ was determined for each.

Radioactivity and carrier in $[^{11}\text{C}]\text{PBR28}$. In each of three glass vials, IS solution (2 ng) in dimethylformamide (DMF; 1 mL) was mixed with $[^{11}\text{C}]\text{PBR28}$ preparation (3–5 μL) and the radioactivity counted with a calibrated γ -counter (model 1480 Wizard; Perkin-Elmer, Waltham, MA). After radioactivity decay, a 50 μL -aliquot of each sample was diluted with 450 μL of 1% acetic acid in aq. acetonitrile (50% v/v), and a sample was injected (5 μL) onto LC–MS/MS. Samples prepared by mixing the IS solution with known concentrations of reference PBR28 (10–0.3125 ng/mL DMF) were analyzed similarly to provide a calibration curve. Except for

the LC column (3 μm ; 2 \times 50 mm; Phenomenex), the LC–MS/MS method used for the quantification of carrier PBR28 was the same as described for the plasma analysis (below).

Arterial blood sampling from human subjects injected with [^{11}C]PBR28. Blood samples used in this study were drawn from human subjects who were recruited by the Molecular Imaging Branch of the National Institute of Mental Health (NIMH). The study was approved by the National Institutes of Health (NIH) Combined Neurosciences Institutional Review Board (NCT 01547780; NCT 01851356; NCT 02233868). The selected participants signed informed consent before entering the study. After [^{11}C]PBR28 injection, arterial blood samples were drawn at 15-s intervals up to 2 min and 30 s, and thereafter at 3, 4, 6, 8, 10, 15, 20, 30, 40, 50, 60, 75 and 90 min. Before injection of the radiotracer, baseline arterial blood was drawn, centrifuged, and plasma used for a control LC–MS/MS (carrier-free) measurement. All methods were performed in accordance with the relevant guidelines and regulations of the NIH.

AIF for [^{11}C]PBR28 by radiometric method. Arterial blood samples were immediately centrifuged after withdrawal and 1.5–2.0 min of transportation. Samples in Eppendorf tubes (cap sealed with Parafilm M) were centrifuged at 1800 g for 2 min. The plasma was transferred to another tube and then split into two portions one for immediate radiometric AIF measurement, based on γ -counting of radioactivity and reverse phase HPLC analysis of plasma, as described previously^{17,26}. Further technical details are provided in Supplementary Information. The second portion of plasma was mixed with IS and stored for separate determination of AIF by LC–MS/MS measurement of carrier PBR28 (see Supplementary Methods for sample preparation).

AIF for [^{11}C]PBR28 by LC–MS/MS quantification of carrier. The MS/MS was tuned as previously described¹⁵ and then set up to monitor m/z 349 $[M+H]^+ \rightarrow 121$ transition for carrier PBR28 and m/z 353 $\rightarrow 125$ for the IS. A sample extracted from plasma (Supplementary Methods) was chromatographed at 40 $^\circ\text{C}$ on a C18 column (Kinetex, 2.6 μm ; 3 \times 75 mm; Phenomenex) eluted at 300 $\mu\text{L}/\text{min}$ with a gradient of binary solvents (A:B) containing ammonium acetate (10 mM), where A was water/acetonitrile (90:10 v/v) and B was acetonitrile/water (90:10 v/v). Elution started with A:B (80:20%) for 0.5 min and continued with a linear gradient reaching A:B (20:80%) over 7 min. The column was then washed for 1 min with B (100%) and then returned to the initial condition. The concentration of carrier PBR28 in plasma was determined from a calibration curve (Supplementary Fig. S4), a plot of reference PBR28 concentration versus peak area ratio for reference PBR28 to the IS. The data were corrected for the skewed ratio of [^{13}C]_i to [^{12}C]_i in carrier PBR28 using the equation $(100+x)/(100+y) \times c$, where x is ratio of [^{13}C]_i to [^{12}C]_i in carrier PBR28, y is the ratio of [^{13}C]_i to [^{12}C]_i in PBR28 (Table 1), and c is the measured concentration of carrier PBR28.

Comparison of different types of AIF measurement for their impact on kinetic modeling. To examine the impact of different types of AIF measurement on the input function for kinetic modeling of PET data, we calculated AUCs (by trapezoidal method) from the LC–MS/MS and radiometric methods (corrected and uncorrected). The resultant AUCs data for eight subjects and their mean \pm SD and relative standard deviation [RSD (%)] were tabulated for each method. Similarities between LC–MS/MS and the radiometric methods were assessed with paired samples t test, test–retest variability (VAR, absolute difference between methods divided by their mean value), Pearson correlation coefficients, and intraclass correlation coefficients (ICC). The data were analyzed using IBM SPSS Statistics for Mac (version 26, copyright IBM Corporation 2019). P values less than 0.05 were considered statistically significant.

Received: 3 March 2020; Accepted: 18 September 2020

Published online: 15 October 2020

References

1. Phelps, M. E. Positron emission tomography provides molecular imaging of biological processes. *Proc. Natl. Acad. Sci. USA* **97**, 9226–9233 (2000).
2. Chua, S. & Groves, A. Biomedical positron emission tomography (PET) imaging. In *Biomedical Imaging: Applications and Advances. Woodhead Publishing Series in Biomaterials* (ed. Morris, P.) 3–40 (Elsevier, Amsterdam, 2014).
3. McCluskey, S. P., Plisson, C., Rabiner, E. A. & Howes, O. Advances in CNS PET: state of the art for new imaging targets for pathophysiology and drug development. *Eur. J. Nucl. Med. Mol. Imaging* <https://doi.org/10.1007/s00259-019-04488-0> (2019).
4. Bar-Shalom, R., Valdivia, A. Y. & Blaufox, M. D. PET imaging in oncology. *Semin. Nucl. Med.* **30**, 150–185 (2000).
5. Pike, V. W. Considerations in the development of reversibly binding PET radioligands for brain imaging. *Curr. Med. Chem.* **23**, 1818–1869 (2016).
6. Heurling, K. *et al.* Quantitative positron emission tomography in brain research. *Brain Res.* **1670**, 220–234 (2017).
7. Slifstein, M. & Abi-Dargham, A. Recent developments in molecular brain imaging of neuropsychiatric disorders. *Semin. Nucl. Med.* **47**, 54–63 (2017).
8. Herholz, K. & Heiss, W.-D. Positron emission tomography in clinical neurology. *Mol. Imaging Biol.* **6**, 239–269 (2004).
9. Villemagne, V. L., Doré, V., Burnham, S. C., Masters, C. L. & Rowe, C. C. Imaging tau and amyloid- β proteinopathies in Alzheimer disease and other conditions. *Nat. Rev. Neurol.* **14**, 225–236 (2018).
10. Volkow, N. D., Fowler, J. S. & Wang, G.-J. Positron emission tomography and single-photon emission computed tomography in substance abuse research. *Semin. Nucl. Med.* **33**, 114–128 (2003).
11. Matthews, P. M., Rabiner, E. A., Passchier, J. & Gunn, R. N. Positron emission tomography molecular imaging for drug development. *Br. J. Clin. Pharmacol.* **73**, 175–186 (2011).

12. Tonietto, M. *et al.* Plasma radiometabolite correction in dynamic PET studies: insights on the available modeling approaches. *J. Cerebr. Blood Flow Metab.* **36**, 326–339 (2016).
13. Zimmerman, B. E. & Cessna, J. T. Development of a traceable calibration methodology for solid $^{68}\text{Ge}/^{68}\text{Ga}$ sources used as a calibration surrogate for ^{18}F in radionuclide activity calibrators. *J. Nucl. Med.* **51**, 448–453 (2010).
14. Lodge, M. A., Holt, D. P., Kinahan, P. E., Wong, D. F. & Wahl, R. L. Performance assessment of a NaI(Tl) gamma counter for PET applications with methods for improved quantitative accuracy and greater standardization. *EJNMMI Phys.* **2**, 11 (2015).
15. Shetty, H. U., Morse, C. L., Zhang, Y. & Pike, V. W. Characterization of fast-decaying PET radiotracers solely through LC–MS/MS of constituent radioactive and carrier isotopologues. *EJNMMI Res.* **3**, 3 (2013).
16. Coplen, T. B. *et al.* Isotope-abundance variations of selected elements (IUPAC technical report). *Pure Appl. Chem.* **74**, 1987–2017 (2002).
17. Briard, E. *et al.* Synthesis and evaluation in monkey of two sensitive ^{11}C -labeled aryloxyanilide ligands for imaging brain peripheral benzodiazepine receptors in vivo. *J. Med. Chem.* **51**, 17–30 (2008).
18. Fujita, M. *et al.* Comparison of four ^{11}C -labeled PET ligands to quantify translocator protein 18 kDa (TSPO) in human brain: (R)-PK11195, PBR28, DPA-713, and ER176—based on recent publications that measured specific-to-nondisplaceable ratios. *EJNMMI Res.* **7**, 84 (2017).
19. Selleri, S. *et al.* 2-Arylpyrazolo[1,5-a]pyrimidin-3-yl acetamides. New potent and selective peripheral benzodiazepine receptor ligands. *Bioorg. Med. Chem.* **9**, 2661–2671 (2001).
20. Zanotti-Fregonara, P. *et al.* Kinetic analysis in human brain of [^{11}C](R)-rolipram, a positron emission tomographic radioligand to image phosphodiesterase 4: a retest study and use of an image-derived input function. *NeuroImage* **54**, 1903–1909 (2011).
21. Christman, D. R., Finn, R. D., Karlström, K. I. & Wolf, A. P. The production of ultra high activity ^{11}C -labeled hydrogen cyanide, carbon dioxide, carbon monoxide and methane via the $^{14}\text{N}(p, \alpha)^{11}\text{C}$ reaction (XV). *Int. J. Appl. Radiat. Isot.* **26**, 435–442 (1975).
22. Gómez-Vallejo, V., Gaja, V., Kozirowski, J. & Llop, J. Specific activity of ^{11}C -labeled radiotracers: a big challenge for PET chemists. In *Positron Emission Tomography—Current Clinical and Research Aspects* (ed. Hsieh, C.-H.) 183–210 (InTech, Rijeka, 2012).
23. MacLeod, A. M. & Reid, J. M. Proton nuclear reaction cross sections in nitrogen at 13 MeV. *Proc. Phys. Soc.* **87**, 437–444 (1966).
24. Zimmerman, B. E., Kubicek, G. J., Cessna, J. T., Plascjak, P. S. & Eckelman, W. C. Radioassays and experimental evaluation of dose calibrator settings for ^{18}F . *Appl. Radiat. Isot.* **54**, 113–122 (2001).
25. Cessna, J. T., Schultz, M. K., Leslie, T. & Bores, N. Radionuclide calibrator measurements of ^{18}F in a 3 ml plastic syringe. *Appl. Radiat. Isot.* **66**, 988–993 (2008).
26. Zoghbi, S. S. *et al.* PET imaging of the dopamine transporter with ^{18}F -FECNT: a polar radiometabolite confounds brain radioligand measurements. *J. Nucl. Med.* **47**, 520–527 (2006).

Acknowledgements

We thank Drs. F.G. Siméon and C. Brouwer for the synthesis of [^{13}C , $^2\text{H}_3$]PBR28 and DPA713, respectively, Drs. J. Hong and S. Telu for the radiosynthesis of [^{11}C]PBR28, and the NIH Clinical PET Department (Chief, Dr. P. Herscovitch) for carbon-11 production. This study was funded by the Intramural Research Program of the National Institute of Mental Health, National Institutes of Health (IRP-NIMH-NIH: ZIA-MH002793; ZIA-MH002795-13).

Author contributions

H.U.S., S.S.Z., and V.W.P. designed the study; H.U.S., S.S.Z., C.L.M., and A.K. performed the research; J.H. and R.B.I. contributed to the data analysis; H.U.S. and V.W.P. wrote the paper. All authors reviewed manuscript content.

Competing interests

The authors declare no competing interests.

Additional information

Supplementary information is available for this paper at <https://doi.org/10.1038/s41598-020-73646-4>.

Correspondence and requests for materials should be addressed to H.U.S.

Reprints and permissions information is available at www.nature.com/reprints.

Publisher's note Springer Nature remains neutral with regard to jurisdictional claims in published maps and institutional affiliations.



Open Access This article is licensed under a Creative Commons Attribution 4.0 International License, which permits use, sharing, adaptation, distribution and reproduction in any medium or format, as long as you give appropriate credit to the original author(s) and the source, provide a link to the Creative Commons licence, and indicate if changes were made. The images or other third party material in this article are included in the article's Creative Commons licence, unless indicated otherwise in a credit line to the material. If material is not included in the article's Creative Commons licence and your intended use is not permitted by statutory regulation or exceeds the permitted use, you will need to obtain permission directly from the copyright holder. To view a copy of this licence, visit <http://creativecommons.org/licenses/by/4.0/>.

This is a U.S. Government work and not under copyright protection in the US; foreign copyright protection may apply 2020